GMP-Overbound Parameter Determination for Measurement Error Time Correlation Modeling

Sandeep K. Jada, and Mathieu Joerger, *Virginia Tech*

BIOGRAPHIES

Dr. Mathieu Joerger obtained a 'Diplôme d'Ingénieur' (2002) from the Ecole Nationale Supérieure des Arts et Industries de Strasbourg, in France, and an M.S. (2002) and Ph.D. (2009) in Mechanical and Aerospace Engineering from the Illinois Institute of Technology in Chicago. He is the 2009 recipient of the Institute of Navigation (ION)'s Bradford Parkinson award, and the 2014 recipient of the ION's Early Achievement Award. Dr. Joerger is currently assistant professor at the Virginia Tech, working on multi-constellation Global Navigation Satellite Systems (GNSS) for safety-critical civilian aviation applications, and on multi-sensor integration, fault detection, and exclusion for highly automated ground vehicle navigation.

Sandeep K. Jada obtained a Bachelor of Technology degree (2008) in Aeronautical Engineering from Jawaharlal Nehru Technological University, Hyderabad, India, and a Master of Engineering degree (2011) in Aerospace Engineering from Indian Institute of Science, Bangalore, India. He worked in Airbus India (2011 to 2018) in the Flight Physics Department, Bangalore, India. He is currently a doctoral student at Virginia Tech working with Dr Mathieu Joerger, with a focus on error time correlation modelling.

ABSTRACT

In this paper, we develop a new method to determine parameter values for high-integrity models of measurement error time correlation. The method builds upon prior research on error correlation modeling, where an upper bound on the estimation error variance is derived given limits on the measurement error variance and correlation time constant. In this paper, we provide the means to derive these limits from experimental data. First, rather than working with autocorrelation functions, we consider "lagged products," which are products of samples taken at different times in a data sequence: we derive a closed form expression of the lagged products probability density function for first order Gauss Markov Processes (FOGMP). These FOGMP models are then used to bound the sample cumulative distribution function (CDF), thereby providing bounds on the mean sample time correlation while accounting for all sample quantiles at all lag times. We illustrate and analyze this approach using simulated and experimental data, and show that it applies even with sparse, unknown (non-GMP) time-correlated data.

INTRODUCTION

This paper describes the design and implementation of a new method to determine measurement error model parameter values for use in time-sequential estimation algorithms that require integrity. Our method complements [1][2] where probabilistic measurement error models over time were derived to achieve high-integrity positioning. In this paper, we provide a method for finding parameter values for these models. We evaluate the method using simulated and experimental GNSS data, which are impacted by multipath errors with uncertain time correlation.

This work is intended for safety-critical navigation operations in aircraft transportation. In such applications, an upper bound on the integrity risk can be predicted to prevent hazardously misleading information (HMI) [3]. If sensor error models are optimistic, then the actual integrity risk is underestimated which can potentially cause HMI. Overbounding theory addresses the measurement error modeling problem for snapshot, instantaneous estimators [4, 5, 6]. But, for Kalman filters or batch (fixed interval) estimators, the measurement error dynamics over time must also be conservatively accounted for.

Over the past five years, approaches have emerged to account for measurement errors over time, which provide guaranteed upper bounds on the positioning error variance for batch estimators in [1] and for Kalman filters in [2]. Both [1] and [2] assume that unknown measurement error time-autocorrelation functions can be upper and lower bounded, for example using two first-

 https://doi.org/10.33012/2020.17137

order Gauss Markov Processes (GMP) with time constants T_{min} and T_{max} and variance σ_{min}^2 and σ_{max}^2. GMPs are convenient bounding functions because they are compatible with Gaussian overbounding and can efficiently be incorporated in linear batch estimators and Kalman filters (e.g., by state augmentation). But [1] and [2] do not address how to find the bounding GMP time constants T_{min} and T_{max}, and variance σ_{min}^2 and σ_{max}^2.

A major issue appears when trying to find hard upper and lower-bounds on actual sensor data using a pair of GMPs: the negative values of empirical autocorrelation functions cannot be lower-bounded by always-positive GMP autocorrelation functions, which are decaying exponentials. For example, empirical autocorrelation functions reaching large negative values can be found for multipath errors in [7] and for orbit and clock ephemeris errors in [8].

In response, in this work, we establish a new method to determine probabilistic upper and lower bounding functions on sample measurement error lagged-product distribution. We show that cumulative distribution function (CDF)-bounding can provide upper and lower bounds on the mean sample lagged product distribution, which are the autocorrelation bounds needed in [1] and [2].

The paper is organized as follows. The second section of this paper describes the context and motivation for this work on measurement error time-correlation modelling. An illustrative example using a batch estimator is discussed. We also explain why overbounding autocorrelation functions is sometimes insufficient, and why a new method is needed. In the third section of this paper, we present a new approach to determine the parameters of bounding GMPs. First, we consider time-lagged product samples, for which we provide a closed-form expression of the probability density function. Then, we outline a step-by-step procedure for finding the parameters of the bounding GMPs. In the fourth section of the paper, the approach is evaluated using simulated sample error data. Error samples are drawn from a single GMP, and then from two GMPs with distinct time constants to show that the proposed method applies to complex, composite error distributions. In the fifth section of this paper, the method is evaluated using ionospheric error free code-minus-carrier data collected in a low multipath environment. This evaluation shows that the method can be applied for bounding the time correlation of actual measurement error data. In the final section, the conclusion and the future work are presented.

PRIOR WORK AND MOTIVATION

The focus of this work is on measurement error time-correlation modelling for sequential, linear estimators used in high-integrity applications. Reference [2] develops a method to model this time-correlation while providing a guaranteed upper-bound on the state estimation error variance. This section gives an overview of the method and of modeling aspects that have yet to be addressed.

Estimation Error Bounding in The Presence of Measurement Error with Uncertain Time-Correlation

For both Kalman filters and batch (or fixed interval) estimators, reference [2] expresses the state estimate error as a linear combination of time-correlated measurement errors. For clarity of explanation, we consider an illustrative example of a least-squares batch estimator that uses a single measurement at time epochs 0 and τ to estimate a current-time state estimate. The current-time state estimation error ϵ_τ can be expressed as:

$$\epsilon_\tau = a_0 \nu_0 + a_\tau \nu_\tau \tag{1}$$

where,

a_0, a_τ are (least squares) estimator coefficients for the current-time state estimate, for measurements at times 0 and τ

ν_0, ν_τ are time-correlated measurement errors at times 0 and τ

We further assume that the measurement errors ν_0 and ν_τ, are outputs of a Markov process that can be written in the following form:

$$\nu_\tau = \rho_\tau \nu_0 + \eta_0 \tag{2}$$

where,

η_0 is a white sequence of driving noise.

τ is the lag time between the measurements.

ρ_τ is the unknown correlation coefficient over the lag time interval τ.

The actual time correlation between ν_0 and ν_τ is unknown, and is equation (2) does not necessarily describe a GMP.

For error modeling purposes, if equation (2) describes a first order Gauss Markov Process (FOGMP), then η_0 is zero mean with variance σ_η^2–The variance of the driving noise σ_η^2 is related to that of the process output variance, noted σ_0^2, via the equation: $\sigma_\eta^2 = \sigma_0^2(1-\rho_\tau^2)$. Using equations (1) and (2), the variance σ_ϵ^2 of ϵ_τ can be derived by taking the expectation of ϵ_τ^2 in equation (1), and can be expressed as:

$$\sigma_\epsilon^2 = (a_0^2 + a_\tau^2)\sigma_0^2 + 2a_0 a_\tau\, \sigma_0^2\rho_\tau \tag{3}$$

If the correlation coefficient ρ_τ is zero, then an upper bound on σ_0^2 guarantees an upper bound on σ_ϵ^2 because the coefficient $(a_0^2 + a_\tau^2)$ is positive. Overbounding theory can be used to determine an upper bound on σ_0^2 [4, 5, 6]. If ρ_τ is not zero and unknown, then upper bounding σ_ϵ^2 depends on whether the cross-product coefficient $a_1 a_2$ is positive or negative. The σ_ϵ^2-bound can then be expressed as:

$$\sigma_\epsilon^2 \le \begin{cases} (a_0^2 + a_\tau^2)\sigma_0^2 + 2a_\tau a_0\, \sigma_{min}^2\rho_{\tau,min} & \text{if,} \quad a_\tau a_0 \le 0 \\ (a_0^2 + a_\tau^2)\sigma_0^2 + 2a_\tau a_0\, \sigma_{max}^2\rho_{\tau,max} & \text{if,} \quad a_\tau a_0 > 0 \end{cases} \tag{4}$$

where $\sigma_{min}^2\rho_{\tau,min}$ and $\sigma_{max}^2\rho_{\tau,max}$ are the lower and upper bounds on the quantity $\sigma_0^2\rho_\tau$. The method described in [2] guarantees an upper bound on σ_ϵ^2 by using an upper bound on $\sigma_0^2\rho_\tau$ ($\sigma_{max}^2\rho_{\tau,max}$) when $a_0 a_\tau$ is positive, and a lower bound on $\sigma_0^2\rho_\tau$ ($\sigma_{min}^2\rho_{\tau,min}$) when $a_0 a_\tau$ is negative. Of course, a more generic example would involve many more terms corresponding to additional sensor measurements at additional sample intervals, with different correlation coefficients ρ_τ depending on lag times, τ, and with cross product terms derived from estimator coefficient being either positive or negative [2].

Reference [11] provides a practical, vectorized approach to implement this process for batch estimators. The method in [2] is powerful because it is proved to work even if the correlation process is not a GMP. FOGMP are used as bounds because they are compatible with overbounding theory, and because FOGMP can easily be incorporated in linear estimators (e.g., by state augmentation in Kalman filters).

For a FOGMP the correlation coefficient can be written as: $\rho_\tau = e^{-\frac{\tau}{T}}$, where, T is the time constant of the process. The upper and lower bounds on measurement error time correlation, $\sigma_0^2\rho_\tau$, can respectively be written as $\sigma_{max}^2 e^{-\frac{\tau}{T_{max}}}$ and $\sigma_{min}^2 e^{-\frac{\tau}{T_{min}}}$. Hence the bounds on the measurement error autocorrelation are parametrized using the four parameters: σ_{min}, T_{min} and σ_{max}, T_{max}.

While it might be intuitive to assume that the $\sigma_{max}^2 e^{-\frac{\tau}{T_{max}}}$ produces the most conservative estimation variance, this is not true in general as shown in [1, 12]. Higher measurement correlation does not always mean that less new information is provided. For example, one may think of velocity estimation as a process of time-differencing position estimates over time; in this case, highly correlated positioning errors are differenced out, yielding more accurate velocity estimates than if errors were not correlated. Therefore, considering an upper bound is insufficient, and a range of time correlation values must be found. Determining this range from data is not addressed in [2].

Limitations of Using Autocorrelation Functions to Bound Correlation Uncertainty

In order determine the FOGMP bounding parameters, a sensible approach is to analyze the sample measurement error autocorrelation function. Let, ν_0 and ν_τ, the measurement errors at times 0 and τ, be the output of a process described by equation (2). The autocorrelation function, $R_\nu(\tau)$, for this process can be written as:

$$R_\nu(\tau) = E[\nu_0\nu_\tau] = \sigma_0^2\rho_\tau \tag{5}$$

where, τ is the lag time between two sample measurement errors, $E[\cdot]$ is the expectation operator. The term $\sigma_0^2\rho_\tau$ is exactly the one we are trying to bound. As described earlier, for a FOGMP, the autocorrelation function, $R_\nu(\tau)$, can be expressed as follows:

$$R_\nu(\tau) = E[\nu_0 \nu_\tau] = \sigma_0^2 e^{-\frac{\tau}{T}} \tag{6}$$

Parameters of the bounding FOGMP functions σ_{min}, T_{min} and σ_{max}, T_{max}. may be determined by analyzing the sample autocorrelation [13]. Unfortunately, this approach does not work in all cases. For example, sample ACFs are shown in [7] and [8] over long lag times for GNSS multipath errors and for satellite orbit and clock, respectively. These ACF curves show negative values, which are impossible to lower bound using a strictly positive decaying exponential.

Another illustration of this issue in given in Figure 1, where we plotted sample ACFs (in grey) obtained using a random number generator for a FOGMP with T = 20 s, and $\sigma_{min}^2 = \sigma_{max}^2 = \sigma_0^2 = 1$. In parallel, theoretical unit-variance ACFs are shown for FOGMPs with T_{min} = 5 s in red and T_{max} = 100 s in blue. Whereas a blue curve can be found to upper bound all sample ACFs, no red curve exists that lower bounds all grey curves because sample ACFs dip below zero for lag times as short as one GMP time constant T.

In the next section, we develop a stochastic approach, not based on ACFs, to find σ_{min}, T_{min} and σ_{max}, T_{max} while accounting for all data samples.

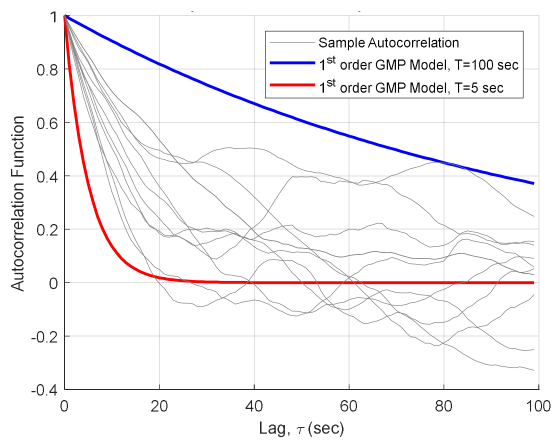

Figure 1: Time correlation bounding example using autocorrelation function, with negative sample autocorrelation.

A NEW MEASUREMENT ERROR TIME-CORRELATION MODELING METHOD

This section aims at finding a range of FOGMP bonding parameters, that can be used to conservatively account for the time correlation affecting all samples in a data set. Instead of working with ACFs, we develop a new method based on "lagged products". A lagged product is a product of sample measurement errors separated in time, which can be written as:

$$P_\nu(\tau) \equiv \nu_0 \nu_\tau \tag{7}$$

where τ is the time lag between two sample measurement errors at times 0 and τ. To facilitate derivations in this section, we define lagged products relative to some fixed initial time, ν_0. The relationship between the lagged product P_ν and the ACF R_ν is expressed in the following equation:

$$R_\nu = E[P_\nu] \tag{8}$$

Figure 2 shows sample lagged products for 10^4 time series plotted as a function of lag time τ, for a FOGMP with time constant T = 10 s and variance $\sigma_0^2 = 1$.

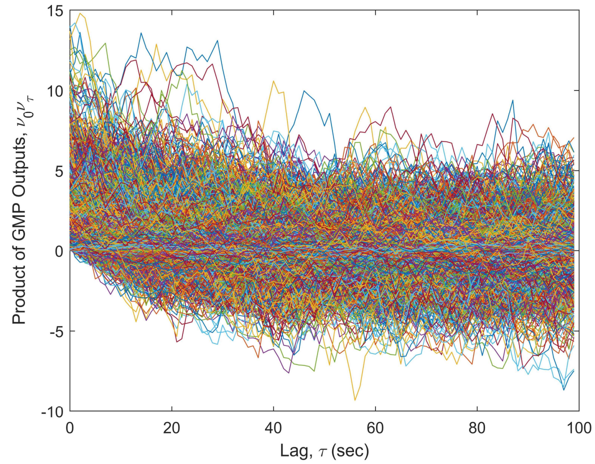

Figure 2: 10,000 time-series of lagged products for FOGMPs with unit variance and time constant T = 10 s.

A key step towards determining FOGMP bonding parameters is to understand the distribution of lagged products $P_\nu(\tau)$. We derived a closed-form expression for the probability density function (PDF) of $P_\nu(\tau)$ for FOGMP based on [9], which provides general solutions for products of correlated standard (zero-mean, unit-variance) Gaussian random variables. For a given τ, the PDF of $P_\nu(\tau)$ can be written as:

$$f_{P_\nu}(z) = \frac{1}{\pi\sqrt{1-e^{-2\frac{\tau}{T}}}} \exp\left(\frac{z\, e^{-\frac{\tau}{T}}}{1-e^{-2\frac{\tau}{T}}}\right) K_0\left(\frac{|z|}{1-e^{-2\frac{\tau}{T}}}\right) \tag{9}$$

where $K_0(\cdot)$ is the modified Bessel function of the second kind of order zero, and we employ the notation 'exp(·)' for the exponential function to improve readability. The term, $e^{-\frac{\tau}{T}}$ is the FOGMP correlation coefficient, ρ_τ, for time constant *T*. It is worth noting that for the non-normalized case where $\sigma_0^2 \neq 1$, we can derive a PDF expression based on [10] as:

$$f_{P_\nu}(z) = \frac{1}{\pi\sigma_\nu^2\sqrt{1-e^{-2\frac{\tau}{T}}}} \exp\left(\frac{z\, e^{-\frac{\tau}{T}}}{\sigma_\nu^2\left(1-e^{-2\frac{\tau}{T}}\right)}\right) K_0\left(\frac{|z|}{\sigma_\nu^2\left(1-e^{-2\frac{\tau}{T}}\right)}\right) \tag{10}$$

For the FOGMP used in Figure 2, we represent the PDF surface for lag times τ ranging from 0 to 100 s in Figure 3. The figure points out that, at zero lag ($\tau = 0$ s), the products $P_\nu(0)$ follow a Chi-Squared distribution with one degree of freedom, which is what we expect for the square of a standard Gaussian random variable. As τ increases, the distribution approaches a modified Bessel function of the second kind of order zero [10].

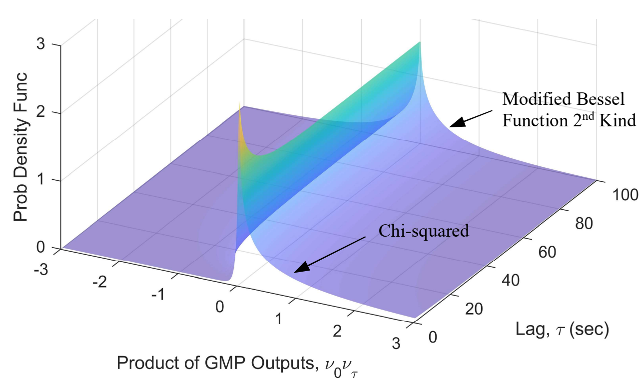

Figure 3: Probability density function for lagged products of a FOGMP with unit variance and time constant T = 10 s.

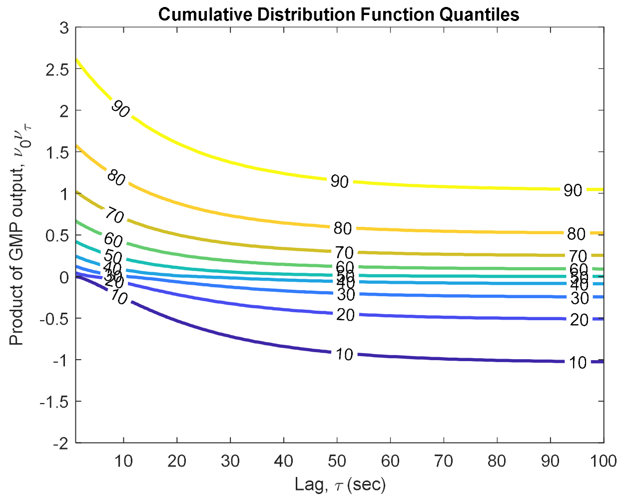

Figure 4: CDF quantiles of lagged product for a FOGMP with unit variance and time constant T = 10 s.

In addition, we can compute the cumulative distribution function (CDF) of lagged products by numerically integrating the PDF in equation (10). The PDF in (10) has an integrable singularity at zero. (In this work, we consider integration intervals with limits around 0+ and 0-. The numerical accuracy achieved with this method is on the order 10^{-16}). CDF quantiles are displayed in Figure 4 for the FOGMP in Figures 2 and 3.

Based on the $P_\nu(\tau)$ CDF, we develop the following five steps procedure to determine T_{min} and T_{max}.

Step 1. Collecting and Partitioning Data

To analyze the lagged product distribution, we need a set of product samples. We consider the case where a time series of samples is collected. For example, in order to evaluate the impact of multipath errors on GNSS signals, we can record ionosphere-free (IF) code minus carrier (CMC) data samples over long time periods [7, 14, 15, 16].

In parallel, we must focus the analysis over a limited range of lag times τ. First, the correlation model only needs to be derived over lag times corresponding to the maximum operational time. Second, if an estimator is used with a fading memory, then the correlation model only needs to be valid over a period where the current-time estimate retains significant knowledge of past-time data, e.g., over twice the smoothing time constant for smoothing filters [17]. Third, measurements separated by more than twice the average correlation time constant may be deemed uncorrelated [18], at which point, the correlation model no longer needs to be accurate. A practical approach is to limit the analysis to τ-values extending to the minimum of these three metrics. To keep this paper generally applicable, we focus on the last criterion, and limit the range of τ's to twice the average correlation time constant.

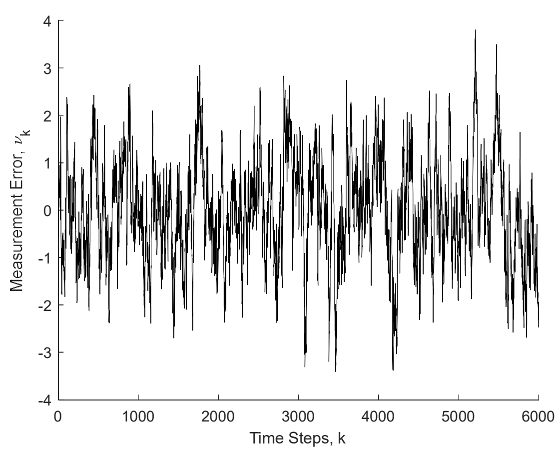

Figure 5: Time series of 6000 simulated samples of a time-correlated random process.

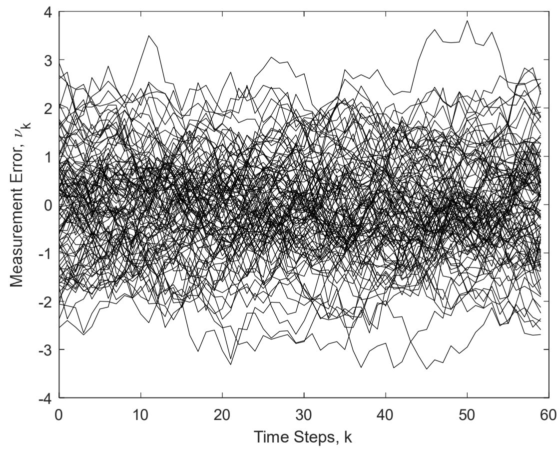

Figure 6: Time segments obtained from slicing up the time series in Figure 5 into 100 regular intervals of 60 samples each.

Thus, if a single large time series is collected, we partition it by extracting time segments of length greater-or-equal to twice the average correlation time constant. As an illustrative example used throughout this section, Figure 5 shows a time series of 6000 samples collected at regular one-second intervals. The time series is sliced in Figure 6 into 100 shorter time segments of 60 seconds each.

Step 2. Determining the Overbounding Variance

We use overbounding theory to find the measurement error model variance σ_0^2 [4, 5, 6]. The process is illustrated in the quantile-to-quantile plot, or Q-Q plot, showing in Figure 7 the sample quantiles versus quantiles of a standard normal distribution. Samples are from the original time series but are taken at twice the average correlation time constant to represent the distribution of uncorrelated samples. Additional considerations to account for the finite number of effectively uncorrelated samples can be found in [8]. In Figure 7, the slope of the overbounding Gaussian CDF represented with a dashed line is 1.1. Thus, whereas the sample variance σ_0^2 is 1 (in units the square of the measurement error's unit), the overbounding variance is $\sigma_{0,OB}^2 = 1.1^2$.

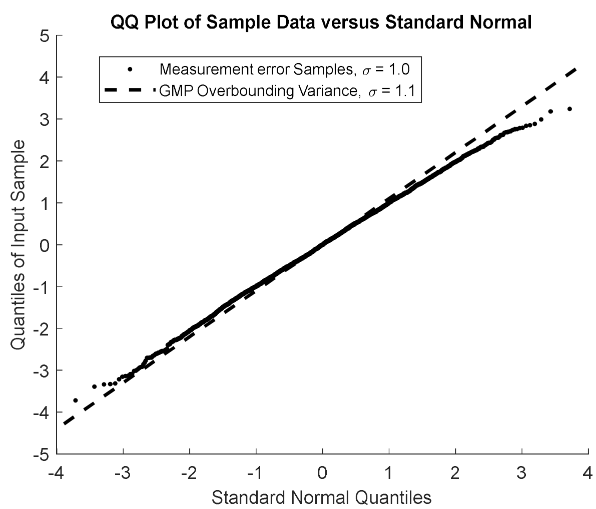

Figure 7: Determining the bounding GMP variance using overbounding theory.

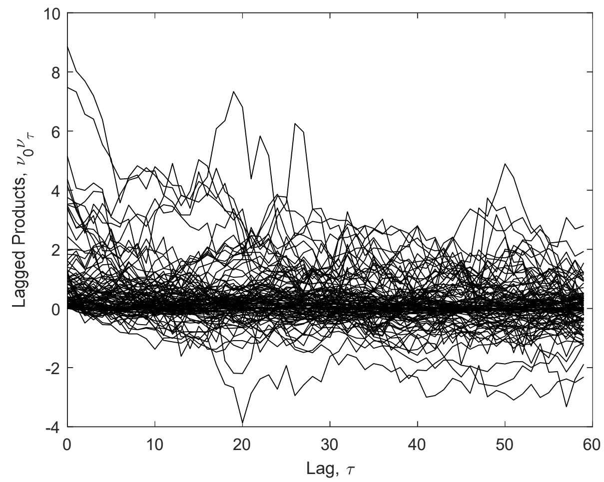

Figure 8: Lagged products of measurements from time segments in Figure 6 as function of lag time τ

Step 4. Evaluating Sample CDFs Over Lag Time

As illustrated in Figure 9, we can evaluate sample CDFs for all values of τ. An alternative representation, not shown here to limit the length of the paper, is the quantile plot in Figure 4 where we can visualize quantiles over all τ's on a single chart.

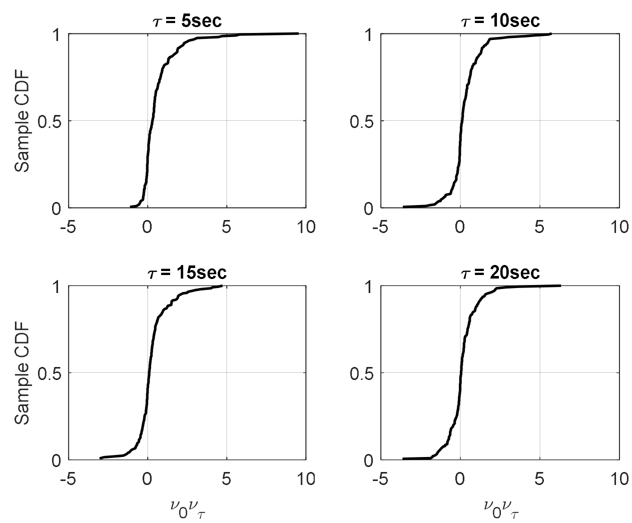

Figure 9: Cumulative distribution function (CDF) of sample lagged products in Figure 8 for four example lag times

Step 5. Upper and Lower-Bounding CDFs To Find Bounding Time Constants and Variances

We can now use the theoretical results obtained in the first part of this section to find two FOGMP CDFs that respectively lower and upper bound all sample CDFs for all values of τ. The motivation for CDF-bounding the sample lagged products distribution using FOGMP models is to determine bounds on the mean of the lagged products, which is the autocorrelation as expressed in equation (5). We make the following statement:

> *The mean of the CDF-upper-bounding distribution lower-bounds the mean of the actual distribution $E[\nu_0\nu_\tau]$. We name it $\sigma^2_{min}\rho_{\tau,min}$.*
> *Similarly, the mean of the CDF-lower-bounding distribution upper-bounds $E[\nu_0\nu_\tau]$. We name it $\sigma^2_{max}\rho_{\tau,max}$.*

The proof of this statement is given in Appendix A.

Figure 10 shows the sample CDF for an example lag time τ, and the two theoretical FOGMP CDFs that lower and upper bound the sample CDF. This must be repeated over all τ values and can be achieved quickly and precisely by switching between the quantile versus τ representation (Figure 4) and the CDFs (as illustrated again in Section 4 of this paper).

Using the bounding parameter values σ_{min}, T_{min} and σ_{max}, T_{max} in the algorithm described in [2] provides an estimation error variance $\bar{\sigma}_{\epsilon}^2$ that is guaranteed to upper bound the sample estimation variance σ_{ϵ}^2 for all time segments in Figure 6.

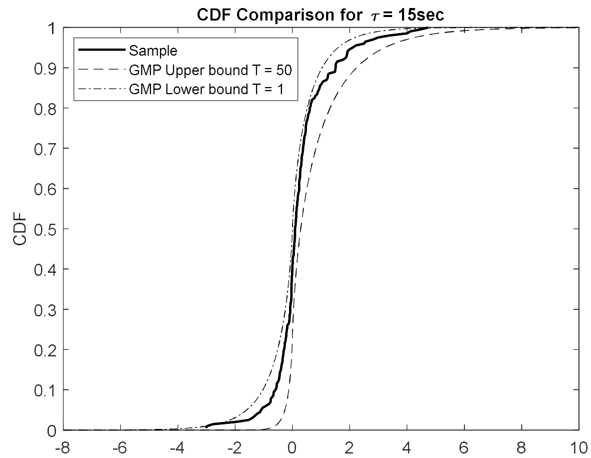

Figure 10: FOGMP upper- and lower-bounding FOGMP lagged product CDFs as compared to sample product CDFs for lag time $\tau = 15s$

EVALUATION OF THE TIME CORRELATION MODELING METHOD USING SIMULATED DATA

In this section, we simulate measurement error data to analyze the time-correlation modeling method derived in Section 3. Two cases are considered.

- **Case 1**: 1000 sample time segments from a FOGMP with T = 10 s, $\sigma_0^2 = 1$.
- **Case 2**: 1000 sample time segments from FOGMPs with two distinct time constants of T = 10 s and T = 3 sec, $\sigma_0^2 = 1$.

Case 1 illustrates the fact that our new method addresses the limitations of using autocorrelation functions to find T_{min} and T_{max} as described in Section 2. It shows that the method can be used even if a sparse set of data is available (which produces a wide range of T_{min} to T_{max}). Case 2 shows that the method can be used when the sample correlation process is complex and unknown, as will be the case using experimental data. The variance of the bounding functions σ_{max}^2 and σ_{min}^2 were taken to be the same in both Case 1 and Case 2.

Case 1 – Modeling Data Drawn from A Single FOGMP

For Case 1, Figure 11 shows the two GMP upper and lower bounding CDFs versus the sample CDF, for example lag times $\tau =$ 1, 3, 5, 10, 15 and 20 s. The GMP upper and lower bounds were obtained for a scaled variance found using Step 2 and for theoretical FOGMP CDFs derived using Step 5 of Section 3. In parallel, Figure 12 shows sample 95%, 68%, 32% and 5% quantiles versus the same quantiles for the upper-bounding FOGMP CDF, for τ values ranging from 0 to 25 s. Figure 13 shows the same curves for the lower-bounding FOGMP CDF.

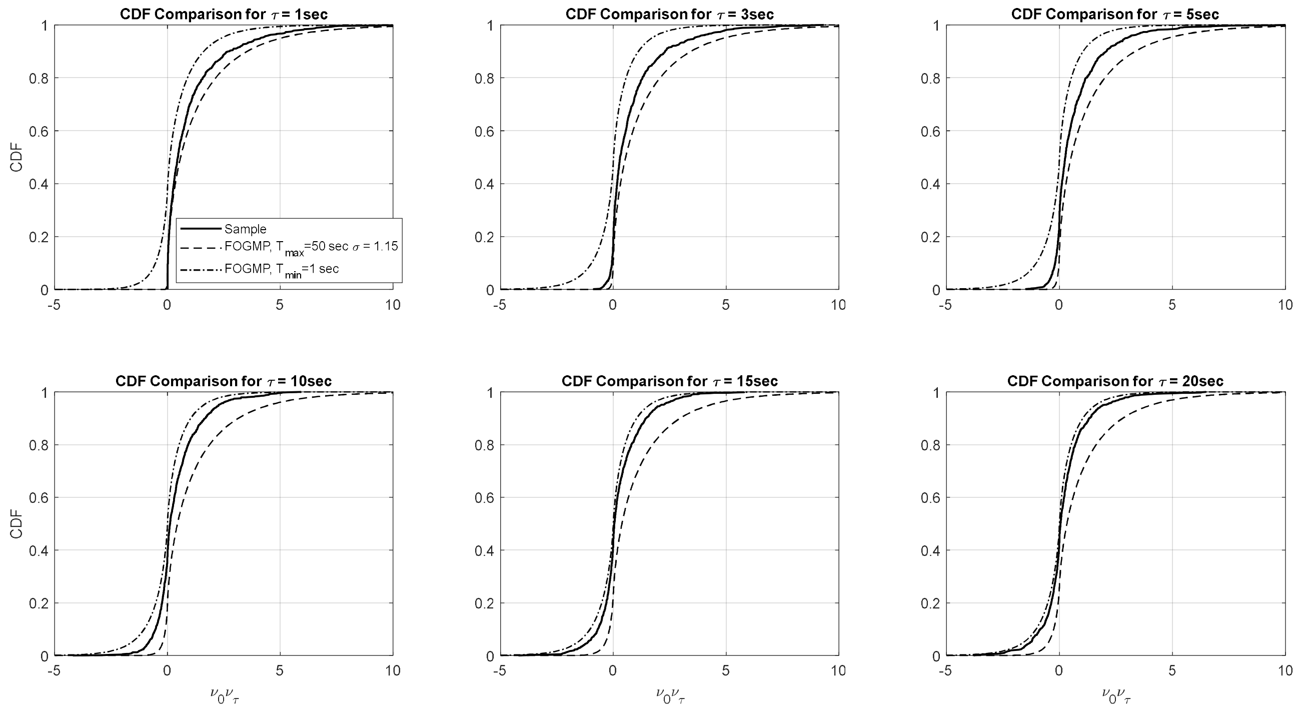

Figure 11: CDF comparison of sample versus FOGMP bounds for Case 1

In Figure 11, the dash-dotted curve (lower-bounding FOGMP CDF) is always above the solid curve (sample CDF) for all values of τ while the dashed curve (upper-bounding FOGMP CDF) is always below. In the representations of Figures 12 and 13, the dashed upper-bounding quantile curves are above the solid sample curves for all quantiles and for all values of τ, whereas the dash-dotted quantile curves are above the solid sample curves for all quantiles and for all values of τ. We used both of these representations to find a time correlation model with time constants ranging from $T_{min} = 1$ s to $T_{max} = 50$ s for Case 1 while setting the standard deviations $\sigma_{min} = \sigma_{max} = 1.15$

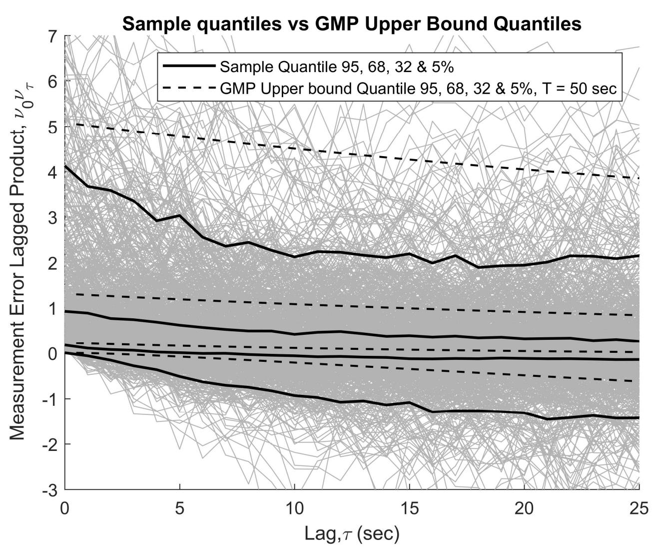

Figure 12: Quantiles over lag time for sample lagged products versus upper-bounding FOGMP model for Case 1

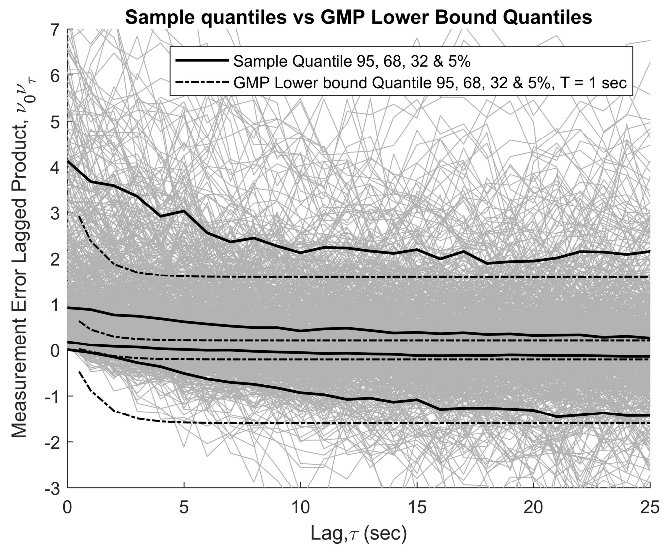

Figure 13: Quantiles over lag time for sample lagged products versus lower-bounding FOGMP model for Case 1

For these values of T_{min} and T_{max}, Figure 14 displays quantiles of both the lower and upper bounding FOGMP models with dash-dotted and solid lines, respectively, for quantiles ranging from 10% to 90% at regular 10% intervals. The spacing between the dash-dotted and solid lines show the area where sample quantiles can live for these values of T_{min} and T_{max} to exist. The method may encounter limitations when the spacing shrinks, i.e., for very small and very large values of τ. Step 1 of Section 3 provides a rationale for limiting the maximum value of τ to twice the average correlation time constant, i.e., 20 s in this case. The models' standard deviations σ_{min} and σ_{max} can be adjusted to address the tightening of the spacing between CDF bounds for small τ's.

In addition, we verified that if we increased the number of samples, then the range of time constants tightens till we approach the values $T_{min} \approx T_{max} = 10$s for the range of quantiles of interest (e.g., from 10^{-5} to 0.99999).

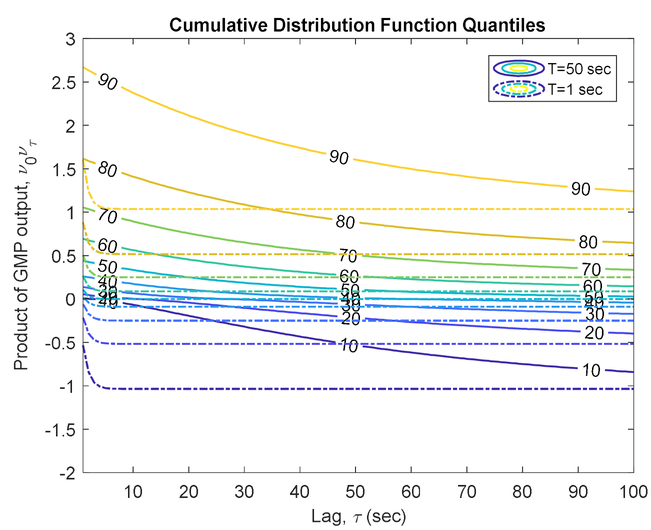

Figure 14: Quantiles versus lag time for two FOGMP with two distinct time constants

This shrinking of the available region for overbounding is the reason of the sample CDFs in Figure 11 and Figure 15 are close for certain quantiles. The lag time 20sec show depleted margins in certain cases.

However, at very short lag times the, the 1 sec, the upper bound is not very effective because we are bounding a chi-squared distribution. The appropriate way to do this would be by inflation of the variance of the upper bounding GMP. The obvious trade-off of this is at large lags, as this would erode the margins at lower quantiles of the upper bound.

Case 2 – Modeling Data Drawn from Two FOGMP With Two Distinct Time Constants

For Case 2, we follow the exact same steps, illustrated in Figures 15 to 17. We found values of time constants ranging from $T_{min} = 0.5$ s to $T_{max} = 50$ s, while setting the standard deviations $\sigma_{min} = \sigma_{max} = 1.15$. This tends to support the fact that, when used in conjunction with the method in [2], the proposed approach can conservatively account for measurement error time-correlation, even when the measurement error correlation is complex (not GMP), and even when the available sample data set is sparse.

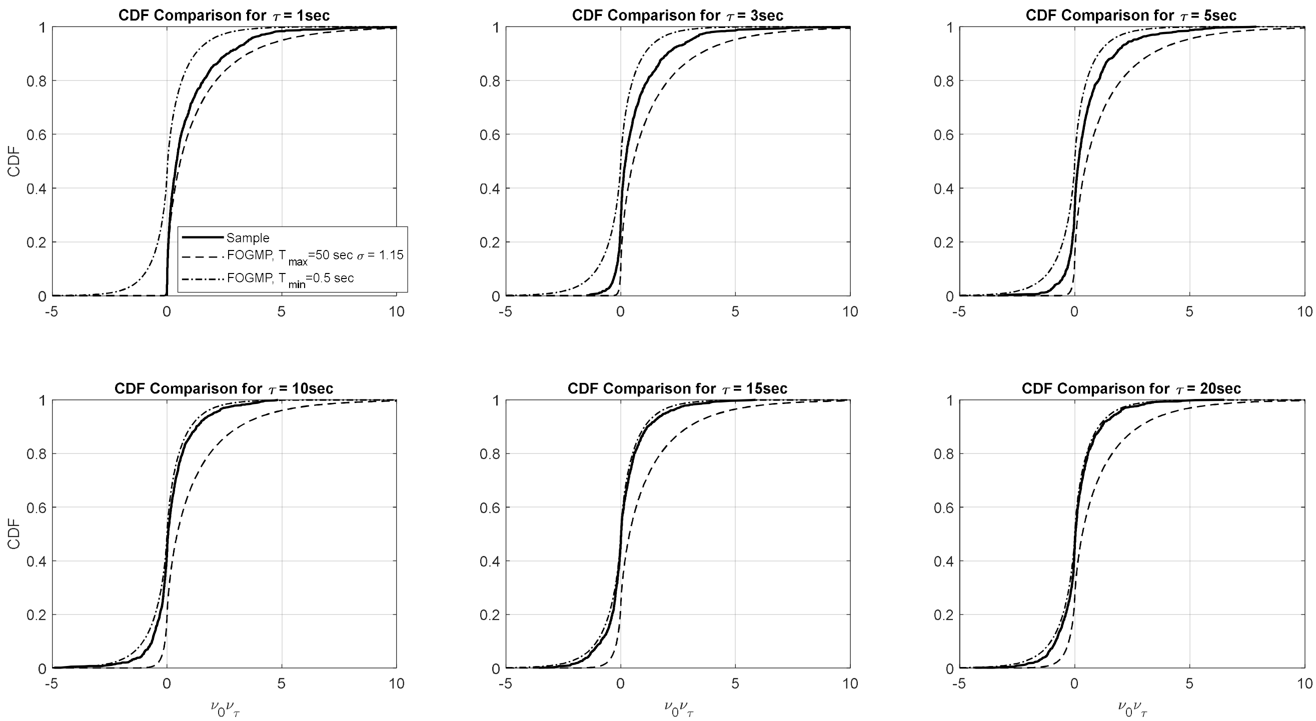

Figure 15: CDF comparison of sample versus FOGMP bounds for Case 2

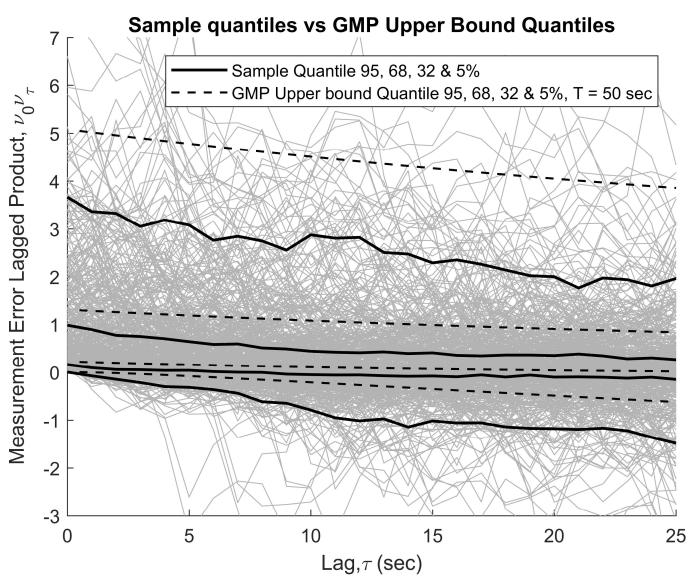

Figure 16: Quantiles over lag time for sample lagged products versus upper-bounding FOGMP model for Case 2

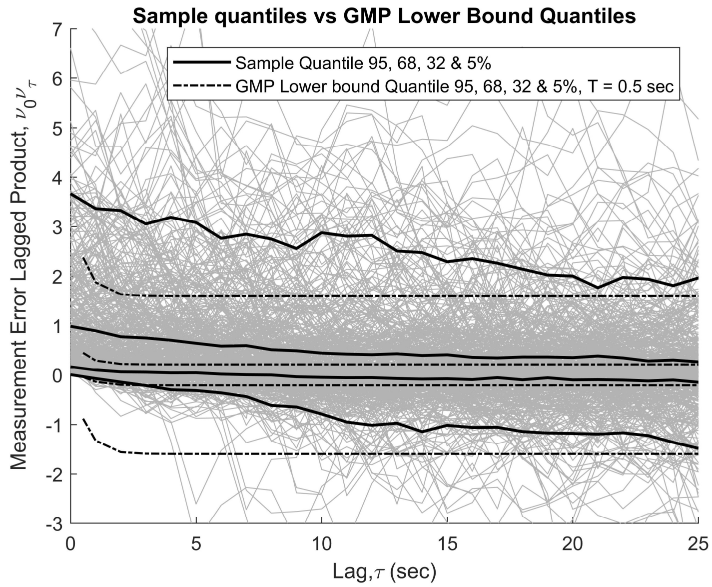

Figure 17: Quantiles over lag time for sample lagged products versus lower-bounding FOGMP model for Case 2

Table 1 summarizes the parameters found from simulated data to model the data sets in Cases 1 and 2. Also, Figure 16 shows that, for the 68% quantile, the sample plot reaching close to the FOGMP bound. Inflating the FOGMP variance would solve this problem, but would then cause the FOGMP 95% quantile in Figure 17 to exceed the sample quantile. There are two elements that would mitigate this issue. One is that we only used 1000 time series. Using a larger number of time series would provide smoother sample quantile curves for quantiles of interest. The other is to consider different variances for the lower and upper bounding FOGMP, as is alluded to in [2] and as is done in the next section.

Table 1: FOGMP Model Parameters

	1st Order GMP Overbounding Parameter		
	T_{max}	T_{min}	σ^2_{min} & σ^2_{max}
Case 1 **T=10 sec, 1000 series**	50 sec	1 sec	1.15
Case 2 **T=3 sec & 10 sec, 1000 series**	50 sec	0.5 sec	1.15

EVALUATION OF THE TIME CORRELATION MODELING METHOD USING EXPERIMENTAL DATA

In this section, the method is evaluated for ionospheric error free code-minus-career (IF CMC) data collected in a low multipath environment in Tucson, Arizona, USA (32°13'36"N 110°56'49"W), on March 1st 2018. The data was collected for 30 GPS satellites over 24 hours. An elevation mask of 10 deg was considered for this data collection. Time-sequences of IF CMC for all 30 satellites are shown in Figure 18. The color code identifies to different satellites. The curves clearly show that the observed multipath error is time-correlated.

The data was collected using a NovAtel ProPak6 GNSS receiver, with a Vexxis GNSS-802 antenna. The receiver was mounted on the roof of a car, which was parked on the roof-floor of a parking garage. Pictures of the equipment are shown in figure 19.

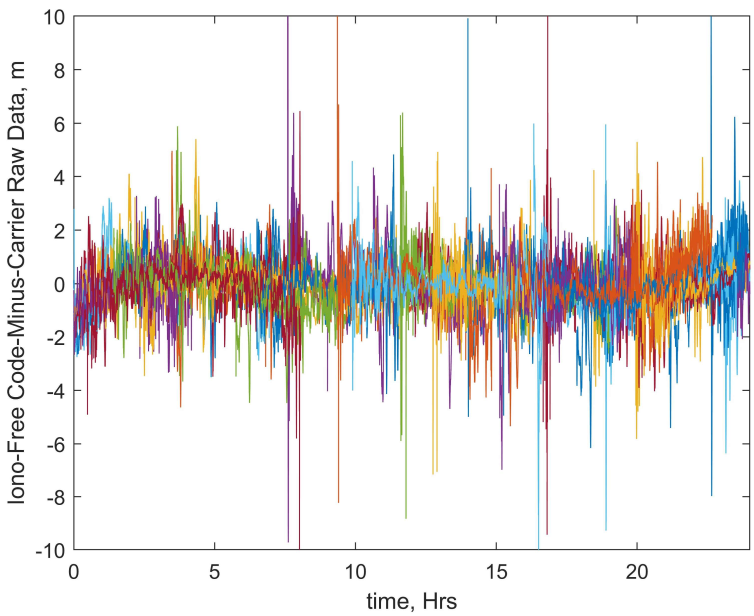

Figure 18: IF CMC data from 32 GPS satellites collected over 24 hours

Figure 19: Testbed Overview: Receiver and antenna are mounted on a parked car in an open-sky area.

The data from each of the 30 satellites was divided into continuous uninterrupted intervals. For each interval, the first and last 300 sec of data were trimmed to remove large variations occasionally observed on low elevation satellites at this location.

The bounding method was then applied to determine the bounds on the time correlation of the IF CMC data. Example CDF bounds are shown in Figure 20 lag times of $\tau = 1s$ to $\tau = 100s$. The bounding FOGMP parameter are: $T_{max} = 1000s$, $\sigma_{max} = 1.5$ and $T_{min} = 5s$, $\sigma_{min} = 0.8$. Future work will seek to determine the limitations of the method, which is how sparse can the data be to still successfully determine FOGMP bounds on time correlation; the structure of the FOGMP sets limits on how much variation over lag-time can be accounted for.

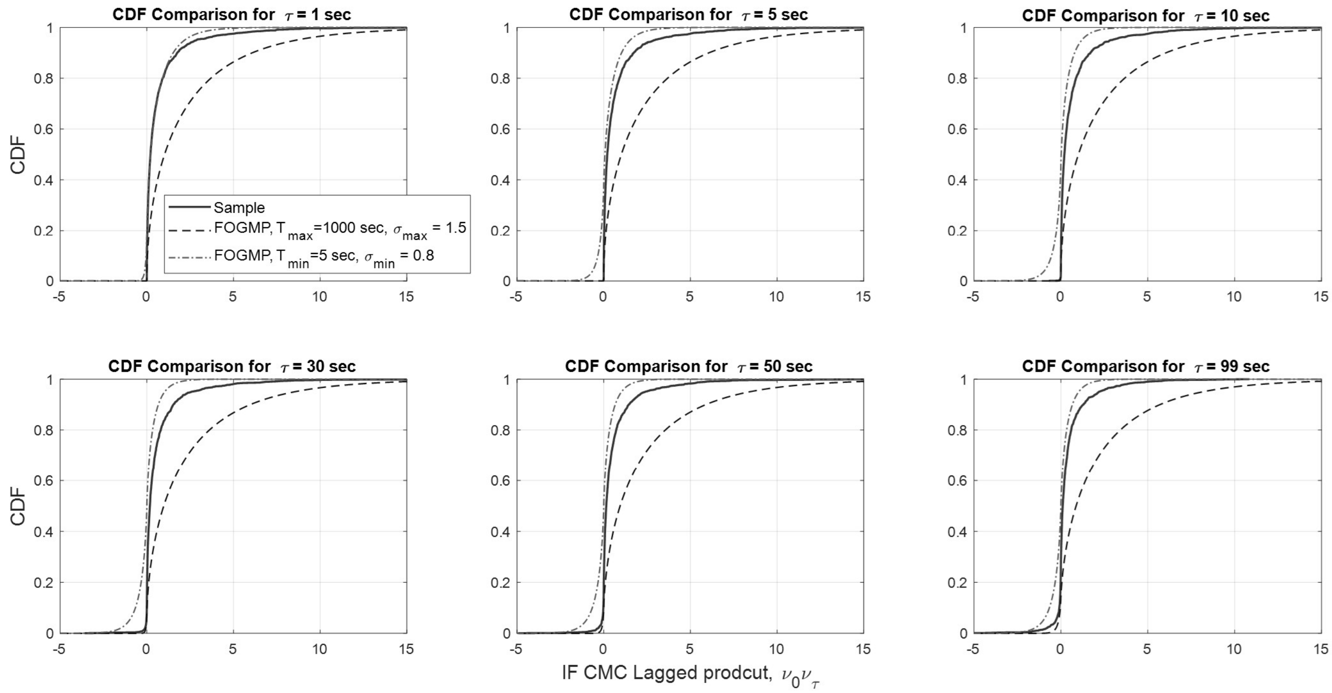

Figure 15: CDF comparison of sample versus FOGMP bounds for IF CMC data

CONCLUSION

In this paper, we develop a new method to determine parameter values for high-integrity measurement error models with unknown time correlation. The method complements prior work in [2], where an upper bound on the estimation error variance is achieved assuming that bounds on the autocorrelation function are given.

This paper provides the means to find upper and lower bounds on the measurement error time correlation coefficients. First, we show that, in general, first order Gauss Markov Process (FOGMP) autocorrelation functions (ACF) are insufficient to directly bound sample ACFs, which can have negative values. Instead, we considered lagged products distributions over varying lag times. We derived a closed form expression of the lagged products probability density function, which we integrated numerically. We then used cumulative distribution function (CDF) bounding to find upper and lower bounds on correlation coefficients while accounting for all sample quantiles at all lag times.

We used simulated data to show that the method could be used even for sparse, unknown (non-GMP) time-correlated data sets. The method was also implemented using experimental GPS data capturing time-correlated multipath errors. The next steps of the work are to derive a formal proof of the conjecture made in the paper, and to determine the limitations of the method when the data is sparse.

ACKNOWLEDGMENTS
The authors gratefully acknowledge the National Science Foundation for supporting this research (NSF award CMMI-1637899). However, the opinions expressed in this paper do not necessarily represent those of any other organization or person.

APPENDIX A: PROOF FOR CDF BOUNDING TO BOUND MEAN

Lemma:

The mean of the CDF-upper-bounding distribution lower-bounds the mean of the actual distribution $E[\nu_0 \nu_\tau]$. Similarly, the mean of the CDF-lower-bounding distribution upper-bounds $E[\nu_0 \nu_\tau]$.

Proof:

A general definition of the expected value of a random variable, X, can be written as:

$$E[X] = \int_{-\infty}^{\infty} x dF(x) \tag{11}$$

where $F(x)$ is the cumulative distribution function (CDF) of the random variable X, represented in Figure 16, and $E[\cdot]$ is the expected value operator.

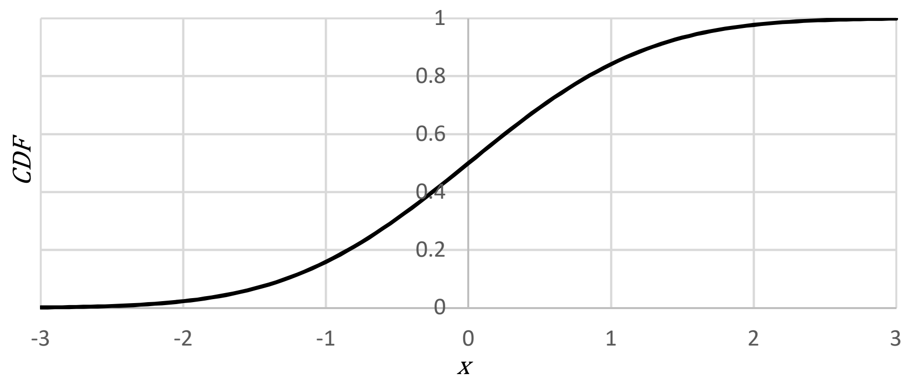

Figure 16: Conventional CDF Representation

Consider a CDF-lower-bounding distribution, $F_L(x)$, on a sample distribution, $F_A(x)$. This lower bound can be written as follows:

$$F_A(x) \geq F_L(x), \qquad \forall\, x \in (-\infty, \infty) \tag{12}$$

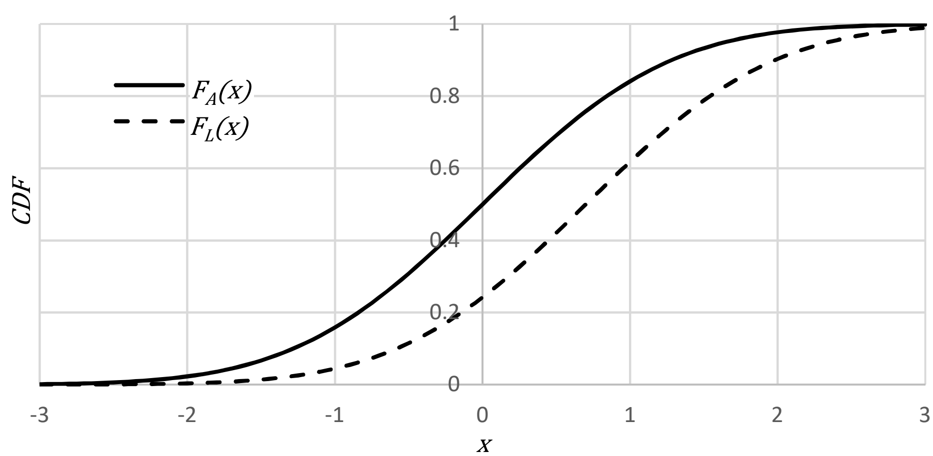

Figure 17: Representation of CDF-lower-bounding

Consider an arbitrary probability value $P \in [0,1]$. Let x_L and x_A respectively be the values of x at which $F_L(x_L) = P$ and $F_A(x_A) = P$. Because CDFs are monotonically increasing functions, we can write the following inequality:

$$x_L(P) \geq x_A(P), \qquad \forall\, P \in [0,1] \tag{13}$$

This is shown graphically in first chart of Figure 18. To obtain Figure 18, we rotated the axes of the CDF curve in Fig. 17 clockwise by 90deg and then flipped about the vertical axis to have positive values of x on top. Using the property of definite integrals, we can integrate the inequality in equation (13) using $F(x)$ as a variable of integration. The following inequality can be written:

$$\int_0^1 x_L(F)\, dF \geq \int_0^1 x_A(F)\, dF \tag{14}$$

By definition of the expected value in equation (11), we have shown that:

$$E[X_L] \geq E[X_A] \tag{15}$$

where $E[X_L]$ is the mean of CDF-lower-bounding distribution and $E[X_A]$ is the expected value of the sample distribution. This proof can also be graphically represented as shown in Figure 18. The shaded regions are the areas under the curves x_L and x_A, which are the expected values of the random variables X_L and X_A. The total area under the curve x_L is more positive than that under x_A, and therefore $E[X_L] \geq E[X_A]$.

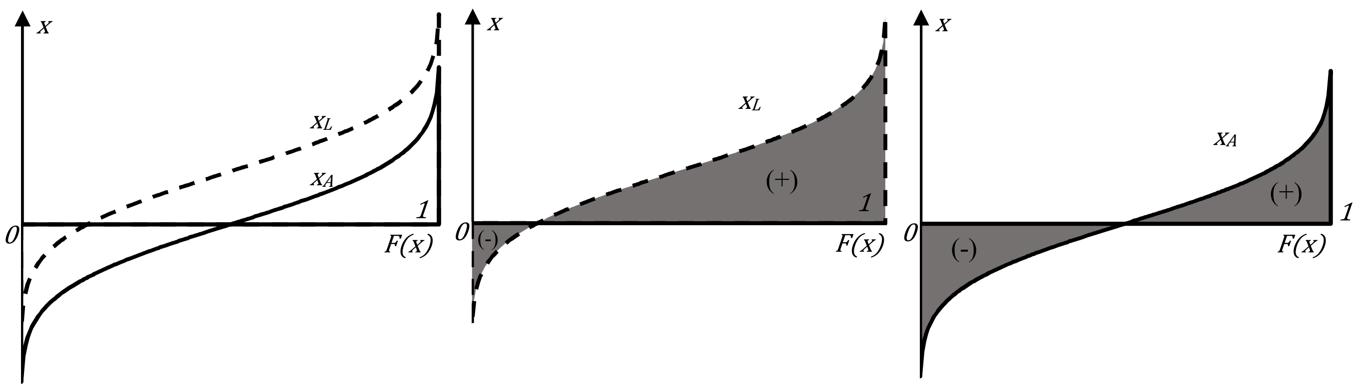

Figure 18: Representation of expected values of CDF lower-bounding distribution and the sample distribution as area under the curves.

We can use the exact same derivation for CDF-upper-bounds, $F_U(x)$, by substituting F_L for F_A, and F_A for F_U. We can write that:

$$\text{if} \quad F_U(x) \geq F_A(x), \qquad \forall\, x \in (-\infty, \infty)$$
$$\text{then} \quad E[X_A] \geq E[X_U] \qquad \blacksquare$$

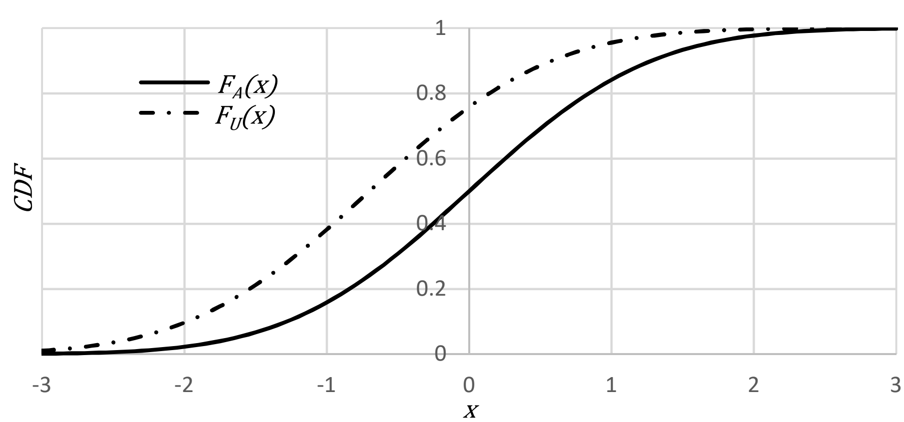

Figure 19: Representation of CDF-upper-bounding

REFERENCES

[1] Langel, S., Joerger, M., and Garcia-Crespillo, O., “Bounding Sequential Estimation Errors Due to Gauss-Markov Noise with Uncertain Parameters,” *Proceedings of the 32nd ION GNSS+ 2019, Miami, Florida, September 2019*.

[2] Langel, S., “Bounding Estimation Integrity Risk for Linear Systems with Structured Stochastic Modeling Uncertainty,” *Ph.D. Dissertation, Illinois Institute of Technology, 2014*.

[3] ICAO, Annex 10, Aeronautical Telecommunications, Volume 1 (Radio Navigation Aids), Amendment 84, published 20 July 2009, effective 19 November 2009. GNSS standards and recommended practices (SARPs) are contained in Section 3.7 and subsections, Appendix B, and Attachment D.

[4] DeCleene, B., "Defining Pseudorange Integrity - Overbounding," *Proceedings of the 13th International Technical Meeting of the Satellite Division of The Institute of Navigation (ION GPS 2000)*, *Salt Lake City, UT, September 2000,* pp. 1916-1924.

[5] Rife, J., Pullen, S., Enge, P. and Pervan, B., "Paired overbounding for nonideal LAAS and WAAS error distributions," in *IEEE Transactions on Aerospace and Electronic Systems*, vol. 42, no. 4, pp. 1386-1395, October 2006.

[6] Blanch, J., Walter, T., Enge, P., "A MATLAB Toolset to Determine Strict Gaussian Bounding Distributions of a Sample Distribution," *Proceedings of the 30th International Technical Meeting of the Satellite Division of The Institute of Navigation (ION GNSS+ 2017), Portland, Oregon, September 2017,* pp. 4236-4247.

[7] Pervan, B., Khanafseh, S., Patel, J., "Test Statistic Auto- and Cross-correlation Effects on Monitor False Alert and Missed Detection Probabilities," *Proceedings of the 2017 International Technical Meeting of The Institute of Navigation*, *Monterey, California, January 2017*, pp. 562-590.

[8] Perea, S. D., “Design of an Integrity Support Message for Offline Advanced RAIM,” *PhD Dissertation, Illinois Institute of Technology, May 2019.*

[9] Nadarajah, S. and Pogany ,T. K., “On the distribution of the product of correlated normal random variables.” *Comptes Rendus Mathematique*, 354(2):201-204, 2016.

[10] Cui, G., Yu, X., Iommelli, S., and Kong, L. “Exact distribution for the product of two correlated gaussian random variables.” *IEEE Signal Processing Letters*, 23(11):1662-1666, Nov 2016.

[11] Racelis, Danielle, Pervan, Boris, Joerger, Mathieu, “Fault-Free Integrity Analysis of Mega-Constellation-Augmented GNSS,” *Proceedings of the 32nd International Technical Meeting of the Satellite Division of The Institute of Navigation (ION GNSS+ 2019), Miami, Florida, September 2019,* pp. 465-484.

[12] Langel, S., Khanafseh, S., Pervan, B., “Bounding Integrity Risk in the Presence of Parametric Time Correlation Uncertainty,” *Proceedings of the 2012 International Technical Meeting of The Institute of Navigation, Newport Beach, CA*, January 2012, pp. 1666-1680.

[13] Gallon, E., Joerger, M., Perea, S., Pervan, B., “Error Model Development for ARAIM Exploiting Satellite Motion,” *Proceedings of the 32nd International Technical Meeting of the Satellite Division of The Institute of Navigation (ION GNSS+ 2019), Miami, Florida, September 2019,* pp. 3162-3174.

[14] Murphy, T., Harris, M., Geren, P., Pankaskie, T., Clark, B., and Burns, J., “More Results from the Investigation of Airborne Multipath Errors,” *Proceedings of the 18th International Technical Meeting of the Satellite Division of The Institute of Navigation (ION GNSS 2005)*, *Long Beach, CA, September 2005*, pp. 2670-2687.

[15] Balaraman A., “Probabilistic Tracking Error Analysis for Automotive Versus Aviation-Grade GNSS Receivers”, *M.S. Report*, The University of Arizona, 2018.

[16] Khanafseh, S., Kujur, B., Joerger, M., Walter, T., Pullen, S., Blanch, J., Doherty, K., Norman, L., De Groot, L., Pervan, B., "GNSS Multipath Error Modeling for Automotive Applications," *Proceedings of the 31st International Technical Meeting of the Satellite Division of The Institute of Navigation (ION GNSS+ 2018), Miami, Florida, September 2018,* pp. 1573-1589.

[17] Chan, F.-C., Joerger, M., and Pervan, B. “Stochastic Modeling of Atomic Receiver Clocks for High Integrity GPS Navigation.” *IEEE Transactions on Aerospace and Electronic Systems*. 50.3. (2014): 1749-1764.

[18] Lawrence, D. “Aircraft Landing Using GPS: Development and Evaluation of a Real Time System for Kinematic Position using the Global Positioning System.” *PhD Dissertation*. *Stanford, CA: Stanford University. (1996)*.